Ice-covered lakes of Tibetan Plateau as solar heat collectors

G. B. Kirillin[1], T. Shatwell[2], L. Wen[3]

[1]Department of Ecohydrology, Leibniz-Institute of Freshwater Ecology and Inland Fisheries (IGB), Berlin, Germany

[2]Department of Lake Research, Helmholtz Centre for Environmental Research - UFZ, Magdeburg, Germany

[3]Key Laboratory of Land Surface Process and Climate Change in Cold and Arid Region, Northwest Institute of Eco-Environment and Resources, Chinese Academy of Sciences, Lanzhou, China

Key Points:

- An abnormal thermal regime under the ice cover of Tibetan lakes is revealed
- The lakes get heated above their maximum density temperature by extremely high level of solar radiation penetrating the ice cover
- The stored heat shortens the ice-covered period and is quickly released into the atmosphere after ice-off, affecting local climate

Corresponding author: G. B. Kirillin, kirillin@igb-berlin.de

Abstract

The Qinghai-Tibet Plateau possesses the largest alpine lake system, which plays a crucial role in the land-atmosphere interaction. We report first observations on the thermal and radiation regime under ice of the largest freshwater lake of the Plateau. The results reveal that freshwater lakes on the Tibetan Plateau fully mix under ice. Due to strong solar heating, water temperatures increase above the maximum density value 1-2 months before the ice break, forming stable thermal stratification with subsurface temperatures > 6 ℃. The resulting heat flow from water to ice makes a crucial contribution to ice cover melt. After the ice breakup, the accumulated heat is released into the atmosphere during 1-2 days, increasing lake-atmosphere heat fluxes up to 500 W m^{-2}. The direct biogeochemical consequences of the deep convective mixing are aeration of the deep lake waters and upward supply of nutrients to the upper photic layer.

1 Introduction

Nicknamed the "third pole", the Plateau of Tibet is the world's largest and highest plateau. It plays a crucial role in the earth's climate and water cycle, for instance in the formation of the Asian monsoon system and as the origin of great Asian rivers such as the Yellow, Yangtze, Mekong, Salween, Brahmaputra, and Indus Rivers [Su et al., 2016]. The Tibetan Plateau is dotted with lakes, which are inherent components of the hydrological cycle driven by the "world's largest water tower".

Due to lack of regular monitoring, the physical regime of the Tibetan lakes remains largely unknown, making it difficult to estimate their contribution to regional-scale energy and mass exchange between land and the atmosphere. Observational data on the physical properties of Tibetan Plateau lakes are scarce and mostly confined to lake surface characteristics obtained by remote sensing [Lin et al., 2011; Zhang et al., 2014]. Moreover, air-lake fluxes measured using eddy covariance methods are too fragmentary to estimate the seasonal variations [Biermann et al., 2014; Li et al., 2015]. Especially little is known about heat transport within the lake water column, in particular, the thermal dynamics under ice. First reports on the mixing conditions and vertical heat transport in Tibetan lakes during the open water seasons were presented only recently [Wang et al., 2014; Wen et al., 2016; Kirillin et al., 2017; Huang et al., 2019], and the winter regime remains largely unexplored.

The lakes on the Tibetan Plateau are ice-covered for 4 to 5 months per year [Kirillin et al., 2017]. The duration of ice cover is determined by heat redistribution in the sediment-water-ice system combined with lateral heat and salt inflows and short-wave radiation under ice. The density stratification created by heat and salt flows under ice can have lasting effects on the subsequent open water season by restricting heat exchange within the water column, and heat and mass exchange between lake and atmosphere. Lakes respond more strongly to global climatic trends than land or oceans due to their high thermal inertia and small size. Accordingly, ice cover and winter dynamics are very sensitive to small changes in the global heat budget [Magnuson et al., 2000].

The importance of the ice covered period for seasonal lake dynamics was only recognized in the last decade [Kirillin et al., 2012]. Modern regional climate models either highly simplify or completely neglect thermodynamics of ice-covered lakes. This produces large errors in estimates of seasonal ice formation and thaw with consequences for the entire regional heat and mass balance in the land-atmosphere system. Development of more sophisticated lake models requires observational data on the thermal regime under ice and its major drivers.

The interactions with the monsoon circulation and global hydrological cycle cause the alpine lakes of the Tibetan Plateau to respond quickly to global changes. Thus first insights into the winter regime of Tibetan lakes are particularly intriguing. We measured the vertical temperature distribution and short-wave radiation flux under ice of the largest freshwater lake of Tibet during the entire ice season of 2015-2016. We observed anomalous warming of the lake water under ice. In the middle of the ice season, warming produced strong convection, which evolved into stable thermal stratification when the temperature exceeded the maximum freshwater density value of ≈ 4 ℃. This caused heat to accumulate in the bulk of the water column accompanied by strong mixing at the water-ice boundary. The thermal regime differs radically from that in the majority of ice-covered lakes, where water temperatures stay below the maximum density value for the largest part of the ice-covered period.

Below, we discuss the driving mechanisms of this specific thermal regime and its importance for the dynamics of the lake system of Tibet.

2 Materials and Methods

2.1 Study site

Ngoring Lake (Fig. 1) is the largest freshwater lake of Tibet (surface area 610 km^2) located in the north-eastern part of the Plateau at 34.5-35.5° N and 97-98° E and belongs to the origin area of the Yellow River. The lake's altitude is ≈4300 m a.s.l., which counts it among the world's highest freshwater lakes. The mean and maximum depths are 17 and 32 m, respectively. Cold semi-arid continental climate prevails in the lake basin, the long-term (1953-2012) monthly mean air temperature varies from 7.7 ℃ in July to −16.2 ℃ in January, with an annual mean of −3.7 ℃ (Li et al., 2015). The lake is oligotrophic, i.e. presumably transparent for short-wave radiation, though according to the early observations of Przhevalsky [Пржевальский, 1888], the Yellow River inflow can produce strong variability in water transparency between the seasons, as well as between the different areas of the lake. The reported lake water transparency (Secchi depth) does not exceed 3 m (Kar 2014). The lake is ice-covered from early December to mid-April.

2.2 Measurements configuration

A chain with 18 RBR T-Solo temperature loggers (declared accuracy 0.002 ℃) was moored in Ngoring Lake on 25 September 2015 at a site with depth of 26.2 m. The temperature loggers were suspended from a float at 1 m intervals to a depth of about 17 m and at 2-3 m intervals below. The uppermost logger was suspended 3.1 m beneath the water surface. During winter, ice thickness grows to more than 0.7 m according to modelling results [Kirillin et al., 2017] and own measurements. Accordingly, the uppermost temperature logger was at a depth of 2.4 m below the ice-water interface during the main winter period. Water temperatures were sampled at 0.1 Hz throughout the entire ice-covered period. Depth was monitored continuously with a pressure sensor at the lake bottom corrected for initial local air pressure. Downwelling short-wave radiation was measured at 10-minute intervals with two cosine-corrected photosynthetically active radiation (PAR, 400-700 nm) sensors (model DEFI2-L by JFE Advantech) moored at depths of 2.4 and 3.6 m, which corresponds to 1.8 and 3.0 m below the ice-water interface.

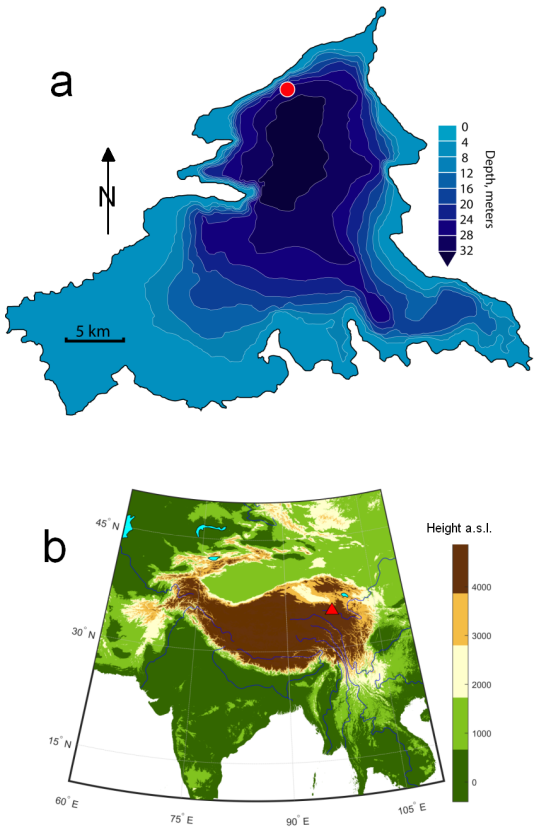

Figure 1. (A) Ngoring Lake bathymetry with location of the mooring station marked by the red circle (B) geographical position of the lake (red triangle). The elevation data are from GLOBE Task Team [1999].

2.3 Vertical heat fluxes

The spectrum of solar (wavelengths range 200-2500 nm) radiation is strongly modified by lake water, which absorbs the long-wave (infrared) part of the spectrum, while yellow substance absorbs the short-wave (ultraviolet) part. As a result, at < 1 m depth, $> 95\%$ of the transmitted radiation falls within the PAR spectral range of 400-700 nm [see e.g. Jerlov, 1976; Leppäranta et al., 2010]. Therefore, the measured PAR values at 2.4 and 3.6 m water depths were adopted as characteristic of the corresponding total downward short-wave radiation flux. We converted the measured quantum irradiance R_q [µmol s^{-1} m^{-2}] to the net downward short-wave radiation I_R [W m^{-2}] using the relationship obtained for ice-covered lakes $R_q/I_R = 4.6$ µmol J^{-1} [see Leppäranta et al., 2010]; the corresponding measurement accuracy in the units of heat flux is ± 3 W m^{-2}. The light extinction coefficient γ and the radiation value at the ice-water interface $_I0$ were determined from a one-band exponential approximation of the short-wave radiation profile $I_R(z)$ in the water column,

$$I_R(z) = I_0 \exp(-\gamma z) \tag{1}$$

The light extinction coefficient was calculated using underwater radiation measurements between 10:00 hr and 14:00 hr.

The vertical "convective" heat flux within the bulk of the water column $Q_{conv}(z,t)$ as function of time t and depth z was estimated from temperatures measured by the thermistor chain $T(z,t)$ using the "flux-gradient method" which adopts the one-dimensional equation of heat transfer, neglecting horizontal advection:

$$C_p \rho \frac{\partial T(z,t)}{\partial t} = -\frac{\partial Q_{conv}(z,t)}{\partial z} - \frac{\partial I_R(z,t)}{\partial z}, \tag{2}$$

where $C_p\rho \approx 4.18 \cdot 10^6$ J K^{-1} m^{-3} is the product of the water heat capacity and density. The solar radiation flux profile $I_R(z,t)$ was recovered from PAR measurements and Eq. (1). Integration of Eq. (2) from a reference depth H, usually chosen close to the lake bottom, to a depth z, and assuming negligible heat flux close to the lake bottom $Q_{conv}(H) \approx 0$, yields the expression

$$Q_{conv}(z,t) = I_R(H,t) - I_R(z,t) - C_p\rho \int_H^z \frac{\partial T(\zeta,t)}{\partial t} \mathrm{d}\zeta, \tag{3}$$

which was solved numerically using finite differences for differentiation and the trapezoid method for integration. Q_{conv} in this formulation is the sum of all "non-radiative"

fluxes including buoyancy-driven convection, small-scale turbulence, and molecular heat conduction.

2.4 Analytical model

In order to analyze the vertical heat transport by radiation and conduction in an ice-covered lake with water temperatures higher than the temperature of maximum density of freshwater $T_m \approx 3.98$ °C, we applied the analytical solution of the one-dimensional heat transfer equation derived by Kirillin and Terzhevik [2011]. The conduction-radiation equation reads as

$$\frac{\partial T(z,t)}{\partial t} - \varkappa \frac{\partial^2 T(z,t)}{\partial z^2} = -\frac{\partial}{\partial z} I_0 \exp(-\gamma z), \tag{4}$$

with the boundary conditions,

$$T(0,t) = 0, \quad T(\infty,t) = T_m, \quad T(z,0) = \phi(z). \tag{5}$$

Here, I_0 is the radiation penetrating the ice normalized by the density and the specific heat of water; γ is the extinction coefficient, assumed to be uniform in the whole daylight spectrum; $\varkappa \approx 1.4 \cdot 10^{-7}$ m^{2}s^{-1} is the thermal diffusivity of water. The first two boundary conditions in (5) are straightforward: the first fixes the temperature of the ice-water interface at the freezing point, whereas the second expresses the fact that the deeper parts of the water column are at the temperature of maximum density T_m and have been completely mixed by preceding convection. Due to the convection the initial temperature profile $\phi(z)$ is homogeneous everywhere except for the "conductive layer" (CL) under ice (red marked part of the temperature profile in Fig. 4a). The temperature profile within the CL can be accurately reproduced by the stationary form of the heat transfer equation, i.e. (4) without the first term on the l.h.s. [Mironov et al., 2002]. Then, the initial profile $\phi(z) \equiv T(z,t)$, is given by

$$\begin{aligned} -\varkappa \tfrac{\mathrm{d}^2\phi(z)}{\mathrm{d}z^2} &= -\tfrac{\mathrm{d}}{\mathrm{d}z} I_0 \exp(-\gamma z) \quad \text{at} \quad z \le \delta, \\ \phi(z) &= T_m \qquad\qquad\qquad\quad \text{at} \quad z > \delta, \end{aligned} \tag{6}$$

and the boundary conditions are

$$\phi(0) = 0, \quad \phi(z)(\delta) = T_m. \tag{7}$$

The solution of (6) is

$$\phi(z) = \begin{cases} \frac{I_0}{\varkappa\gamma}(1 - \mathrm{e}^{-\gamma z})(1 - \frac{z}{\delta}) + T_m \frac{z}{\delta} & \text{at} \quad 0 < z < \delta, \\ T_m & \text{at} \quad z > \delta. \end{cases} \tag{8}$$

The thickness of the layer δ can be found from the additional condition $\partial T/\partial z = 0$ at $z = \delta$. This leads to an algebraic equation for δ as function of the mixed layer temperature T_m, I_0 and γ [Barnes and Hobbie, 1960]

$$\varkappa(T_m - T_f) + \delta I_0 \mathrm{e}^{-\gamma\delta} + \gamma^{-1} I_0 \left(\mathrm{e}^{-\gamma\delta} - 1\right) = 0 \tag{9}$$

The non-homogeneous heat transfer PDE problem (4) is closed through the conditions (8)-(9) and can be solved analytically, assuming the solar heat flux I_0 is constant in time. The final solution is

$$T(z,t) = \left\{T_m - \frac{I_0}{\varkappa\gamma}\right\}\left\{\widetilde{z} + \frac{1}{2}\Big[\mathrm{erfc}_1(x) - \mathrm{erfc}_1(y)\Big]\right\}\widetilde{\delta}^{-1} + \frac{1}{2}\frac{I_0}{\varkappa\gamma}\left\{\widetilde{\delta}^{-1}\mathrm{e}^{-\gamma\delta}\left(\Big[\mathrm{erf}(x) + \mathrm{erf}(y)\Big]\widetilde{z} + \Big[\mathrm{e}^{-x^2} - \mathrm{e}^{-y^2}\Big]\pi^{-1/2}\right) + \mathrm{e}^{\widetilde{\gamma}^2 - \gamma z}\mathrm{erfc}(y + \widetilde{\gamma}) - \mathrm{e}^{\widetilde{\gamma}^2 + \gamma z}\mathrm{erfc}(x + \widetilde{\gamma}) - 2\mathrm{e}^{-\gamma z} + 2\right\}, \tag{10}$$

where $\widetilde{z} = z/\sqrt{4\varkappa t}$, $\quad \widetilde{\delta} = \delta/\sqrt{4\varkappa t}$, $\quad \widetilde{\gamma} = \gamma\sqrt{\varkappa t}$,

$$x = (\delta + z)/\sqrt{4\varkappa t}, \quad y = (\delta - z)/\sqrt{4\varkappa t}.$$

Here, erf, erfc and erfc_1 are the error function, the complimentary error function and the first order iterative complimentary error function, respectively [see e.g. Carslaw and Jaeger, 1959]. The derivative of eq. (10) with respect to z can be used to calculate the heat flux at the ice-water interface ($z = 0$), which is given by

$$\varkappa\frac{\partial T(0,t)}{\partial z} = \frac{I_0}{\gamma\delta}\left\{\gamma\delta\ \mathrm{e}^{\gamma^2 t\varkappa}\,\mathrm{erf}\Big(\frac{\delta + 2\gamma t\varkappa}{2\sqrt{t\varkappa}}\Big) - \gamma\delta\,\mathrm{e}^{\gamma^2 t\varkappa} - \mathrm{erf}\Big(\frac{\delta}{2\sqrt{t\varkappa}}\Big) + \mathrm{erf}\Big(\frac{\delta}{2\sqrt{t\varkappa}}\Big)\mathrm{e}^{-\gamma\delta} + \gamma\delta\right\} + \mathrm{erf}\Big(\frac{\delta}{2\sqrt{t\varkappa}}\Big)\frac{\varkappa T_m}{\delta} \tag{11}$$

3 Results

3.1 Surface cooling and ice formation

According to the water temperature data, the ice cover formed at the lake surface on 12 Dec ± 1 day. Here, we used the evidence of the sudden drop in the latent and sensible heat release at the lake surface after the ice cover formation [Kirillin et al., 2012]. As a result, the water column quickly ceased cooling and the mean temperature began to rise when the entire lake surface froze (see the temperature

minimum at the "ice-on" mark in Fig. 2). Similarly, the moment of the "ice-off" was identifiable in the water temperature data by a sudden drop of the mean water temperature to the maximum density value T_m on 18 Apr (Fig. 2). The total ice-cover duration was 126 days.

Prior to formation of the ice cover, cooling at the lake surface continued for several weeks at a nearly constant rate of 0.2 °C day^{-1}, which corresponds to a net heat loss from a 17 m deep lake of $>$ 150 W m^{-2}. The water column started to re-stratify around 24 Nov, when the water temperature dropped below T_m (Fig.2) changing the sign of the surface buoyancy flux to positive and cancelling thereby convection. However, at depths above the mean depth of the lake, the water column remained nearly thermally homogeneous, indicating surface mixing by strong winds, typical for the Tibetan Plateau, which destroy the near-surface stratification. As a result, at the moment of ice formation, the entire 26 m deep water column cooled down to $<$ 1 ℃. Such a strong cooling rarely occurs in lowland freshwater lakes, where stable stratification at temperatures below T_m develops near the lake surface and decelerates the cooling of the bulk of the water column. It took only about 3 weeks for the surface temperature of the lake to cool from T_m to the freezing point and the stable stratification at the begin of the ice-covered period did not exceed 1 ℃over 20 m of the water column.

3.2 Convection by solar radiation at temperatures below T_m ("Normal winter")

Because of the weak stratification at the moment of ice formation, a thermally-homogeneous convective layer quickly developed driven by absorption of under-ice solar radiation in the upper part of the water column. In early January, only 20 days after the ice cover formation, the convective mixed layer achieved the mean depth of the lake (~17 m). Afterwards, the character of mixing changed: the gradual water temperature increase was superimposed by irregular short-term oscillations with characteristic time scales of a few days (Fig. 2). Heat intrusions at water depths beneath 17 m were clearly identifiable by repeated temperature increases of several tenths of a Kelvin throughout January, with the strongest one lasting from 27 Jan to 12 Feb (Fig. 2). The upper waters revealed in turn short-term temperature drops, which were destroyed within 1-2 days by continuous heat supply from the solar radiation absorption. After 12 Feb, 2 months after ice-on, free convection mixed the

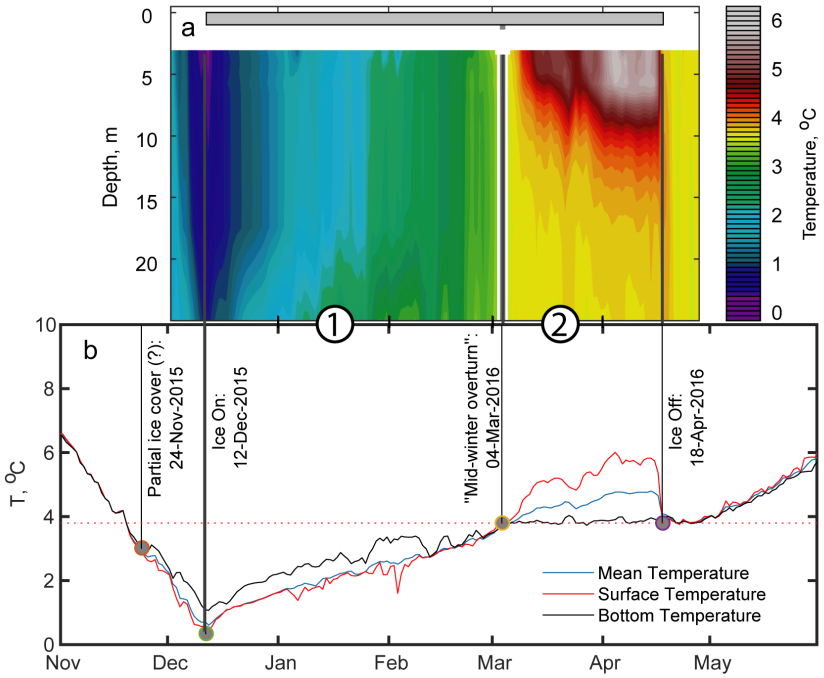

182 Figure 2. Succession of mixing states in the ice-covered season of Ngoring Lake as revealed by
183 the mean water temperature and its vertical gradient.

212 entire 26 m deep water column at the observational site, but several warm intrusions
213 intermittently restored the near-bottom stratification. The temperature pattern is
214 characteristic of advective heat transport from the warmer shallow littoral to the
215 deep central part of the lake by downslope density currents with upwelling of colder
216 water into the convective layer by transient residual currents [Kirillin et al., 2015].
217 Eventually, on 04 Mar, the water column warmed up to T_m and was fully homoge-
218 nized by convective mixing.

219 3.3 Strong heating and inverse stratification under ice ("Anomalous winter")

220 As soon as the water temperature beneath the ice achieved T_m, the free convec-
221 tion was halted, and stable vertical stratification developed in the bulk of the water
222 column. Here, a distinct 3-layer vertical structure was created by the interplay of
223 the volumetric heating by radiation absorption and the upward heat release at the
224 ice base. The radiation absorption depresses convection and produces stable strati-
225 fication with downward temperature decrease in the bulk of the water column, akin

to formation of the summer stratification. On the other hand, the heat release from the water column to the ice cover produces an upward decrease of the water temperature near the ice–water interface. This resulted in a subsurface temperature maximum in the uppermost part of the water column covered by measurements, with temperatures growing continuously until the ice broke up in mid-April, when temperature values beneath the ice cover exceeded 6 ℃(Fig. 2). The fixed temperature $T_f = 0\,℃$ at the ice base requires a thermally stable interfacial layer with temperatures increasing downwards from T_f and T_m to exist immediately under ice. This uppermost layer apparently did not exceed 1 m in thickness and was too thin to be covered by the moored sensors. The thermally unstable "inversion" layer with temperatures decreasing upwards from its maximum to T_m (see the schematic temperature profile Fig. 4b) was also not completely covered by the measurements. The modeling results (see below) and the temporal variability in the upper part of the measured temperature profiles suggest the thickness of the "inversion" layer to vary within 1-2 meters due to diurnal variations in solar radiation and the resulting convection.

Ice began to break up at midday on April 16 and had thawed completely within 36 h. During this 36 h period, the temperature within the near-surface peak decreased from 5.8 ℃ to 3.8 ℃. The corresponding drop of the mean lake temperature from 4.7 ℃ to 3.8 ℃was equivalent to an average heat loss flux from the lake surface of up to 500 W m^{-2}.

3.4 Under-ice solar radiation

Underwater radiation measurements showed that the extinction coefficient γ = 0.25 m^{-1}. Using the extinction coefficient and the Lambert-Beer law, we estimated the radiation at the ice-water interface from the measurements at the depth of the sensors. The mean downward radiation at the ice-water interface was 42.2 W m^{-2} during the "normal" winter, and 46.5 W m^{-2} during the "anomalous" winter. The mean solar radiation reaching the ice-surface during these periods was 171 and 280 W m^{-2}, respectively, according to the ERA5 reanalysis [Hersbach et al., 2020]. Considering that the visible band (400 - 700 nm) accounts for about 45% of broadband solar radiation on the Tibetan Plateau [Li et al., 2010], roughly 55% of visible radiation penetrated the ice cover during the normal winter, and about 37% during the

anomalous winter. This suggests little snow cover, especially during the earlier ice cover period, and an increase in light attenuation as the ice cover matured. Overall, this strong radiative warming suggests that all lakes on the Tibetan Plateau heat to above 4 ℃during the ice-covered period.

3.5 Modeling results

To analyze mixing conditions during the "anomalous winter" we fitted the model (10) using the measured solar radiation I_0 and extinction coefficient γ to the measured temperature profiles and obtained the estimation of the thermal diffusivity under ice $\varkappa = 1.41 \cdot 10^{-6} \pm 4.6 \cdot 10^{-8}$ m^2 s^{-1}. The model described the observed daily mean temperatures well with a root mean square error of 0.19 ℃ and bias of 0.012 ℃ (Fig. 3).

Since the radiation-diffusion model assumed a stationary radiation flux and neglected gravitational instability, it did not capture the diurnal temperature variations and the development of the nearly homogeneous vertical temperature distribution in the upper part of the measured temperature profiles created by convective mixing in the "inversion" layer (Fig.3d). However, the model adequately reproduced both the strength of the subsurface temperature peak and the shape of the temperature profile in the stably stratified water column beneath, indicating the simple radiation-diffusion balance to hold true in the bulk of the water column. It is worth noting that the fitted value of the vertically-constant diffusion $\varkappa = O(10^{-6})$ m^2 s^{-1} is an order of magnitude higher than the molecular value, suggesting additional mixing mechanisms contributed to the vertical heat transport, such as breaking of internal waves in the stably stratified water column. Using Eq. (11), the model suggested that the heat flux from the water to the ice was on average 22.3 W m^{-2}. In reality this heat flux can be much higher due to strong mixing under the ice caused by secondary convection, which the model does not account for.

3.6 Heat budget

The critical differences in the heat budget of the lake water column for the "normal" and the "anomalous" winter are distinguishable in the mean profiles of the vertical heat flux during both periods (Fig. 4) calculated from Eq. (3). In the first

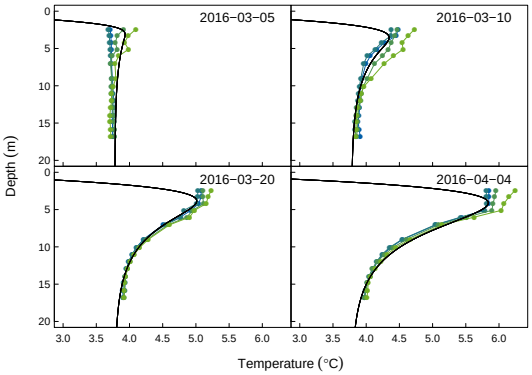

Figure 3. Modeled (black solid lines) and observed (lines with symbols) temperature profiles during the period of inverse stratification. The observed profiles are 4-hour averages on the given calendar day.

period, the profile of the total flux $Q_{conv} + I_R$ is linear, corresponding to the homogeneous vertical temperature distribution produced by convective mixing. At the upper boundary of the water column covered by the measurements (water depth $\approx$ 3 m), the downward flux is around 6 W m^{-2}. Using this value as a boundary condition and taking into account the fixed temperature of 0℃ at the ice-water interface, application of Eq. (3) to the layer $0-3$ m yields the estimation of the mean flux at the ice base as ≈ -13 W m^{-2}. In the second period, after formation of the stable density stratification, the downward heat flux dropped significantly in the bulk of the water column (Fig. 4b), and changed its sign to negative (upward) at 3-6 m water depth. The boundary value of -7 W m^{-2} at 3 m depth, when substituted to Eq. (3), results in the ice base heat flux of ≈ -29 W m^{-2}, which is about 1/3 higher than the estimate obtained with the analytical model above.

4 Discussion

Our results elucidate novel aspects of the thermodynamics of alpine ice-covered lakes that are particularly relevant not only to their behavior as aquatic ecosystems, but also to the role that the world's largest high-mountain lake system—the Qinghai-Tibetan Plateau—plays in the land-atmosphere interaction. The combined effect of strong solar radiation and the cold atmosphere produces cardinal differences between ice-covered Tibetan lakes and lowland high-latitude freshwaters in terms of the thermal and radiation regime.

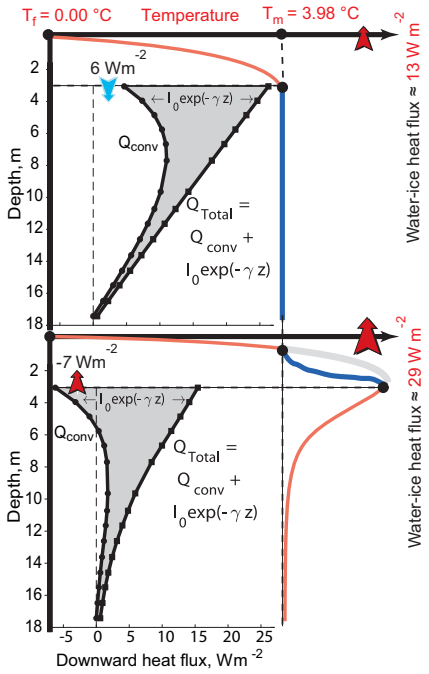

Figure 4. Mean vertical heat fluxes (lines with dots) and schematic temperature profiles (solid lines) during (a) the convective period and (b) the stratified period.

The most striking feature of the observed thermal structure is the heating of the water column up to the maximum density value several weeks before the ice breakup. Early limnological studies [Rossolimo, 1929; Koźmiński and Wisznewski, 1934] reported the phenomenon of anomalous heating of ice-covered freshwater lakes up to temperatures exceeding T_m followed by a "temperature dichotomy" with a sub-surface temperature maximum. However, the situation was rather short-lived, appearing just days before the ice breakup and resulting in strong acceleration of the ice cover melt [Mironov et al., 2002; Kirillin and Terzhevik, 2011].

Both high transparency of the oligotrophic lake water and dry thin atmosphere determine the particular role of the short-wave solar irradiance I_R in the heat budget of alpine lakes. The surface value of total (direct and diffuse) I_R at heights of the Tibetan Plateau is close the no-atmosphere values [Li et al., 2015, 2000]. As a result, a high amount of solar radiation penetrates the snow-free ice cover and is stored distributed across the transparent water column. On the other hand, the strong heat loss from the ice surface prevents ice melt and release of the heat accumulated in the water back to the atmosphere. The strong surface heat loss also ensures low

heat content and weak stratification of the water column at the moment of ice-on as compared to the non-alpine ice-covered lakes, where dense warm waters with temperatures $\lesssim T_m$ typically accumulate near the lake bottom [Bengtsson and Svensson, 1996; Kirillin et al., 2012]. Weak thermal stratification additionally contributes to the quick penetration of the convective mixing into the water column after the ice-on: Lake Ngoring was mixed down to its mean depth within less than a month, and, assuming the observed conditions as typical for freshwater Tibetan lakes, convection would completely mix any lake with total depth of $\lesssim$ 100 m during the 4 months of the ice-covered period.

Another remarkable feature of convective mixing in Tibetan lakes indirectly evidenced by our results is the strong horizontal heat exchange during the later stage of the convective period. As soon as the mixed layer depth exceeds the mean lake depth, a significant shallow part of the lake gets mixed by convection to the bottom and starts to warm faster than the deeper pelagic areas, where the solar energy is fractionated between the mixed layer warming and convective entrainment into the stratified water column. As a result, warm dense waters sink along the bottom slope, increasing the thermal stratification in the central part of the lake and contributing simultaneously to homogenization of the water column, as exemplified by the temperatures observed in late February (Fig. 2). The effect has been previously reported at the concluding stage of the ice-covered period in high-latitude lakes [Kirillin et al., 2015], but may contribute much more strongly to mixing of alpine lakes due to the stronger solar heating and, as a result, higher lateral temperature gradients lasting for a significant part of winter.

The "anomalous" winter with under-ice water temperatures exceeding the maximum density value lasts in Tibetan lakes for more than a month, or about one third of the entire ice-covered period. Consequently, the thousands of lakes of the Qinghai-Tibet Plateau act as "lenses" spotted around the landscape and accumulating solar heat in a thin subsurface layer under ice. The heat stored under lake ice accelerates the ice melt: our estimations of the water-ice heat flux of 10-30 W m^{-}2 are about an order of magnitude higher than estimates from temperate and polar lakes [Bengtsson and Svensson, 1996; Jakkila et al., 2009; Kirillin et al., 2018]. Immediately after the ice breakup, the heat is released to the atmosphere within 1-2 days, creating "hot spots" in land-atmosphere interaction with strong upward heat fluxes of $\tilde{5}$00 W m^{-}2,

which are several times higher than those from the surrounding land [Li et al., 2015; Wen et al., 2016]. The resulting effects on the atmospheric boundary layer include strong horizontal temperature differences, intensification of convection driven by surface heat flux, and strong water mass flux into the atmosphere. Taking into account the large lake-covered area of the Qinghai-Tibet Plateau and importance of its water budget, the cumulative lake effect is regional or even global rather than local. It is important to mention the potential biogeochemical and ecological projections of the specific mixing and temperature regime. The full mixing by convection of the entire water column in mid-winter ensures supply of the dissolved oxygen to the near-bottom layers, suggesting the Tibetan lakes are much less prone to winter hypoxia typical for small ice-covered lakes in higher latitudes [Golosov et al., 2007; Terzhevik et al., 2009]. The high amount of subsurface radiation is in turn favorable for under-ice plankton primary production, while relatively warm conditions in the subsurface temperature maximum stimulate microbiological activity. Particularly the deep convective mixing, which brings deep nutrients to the surface, followed by formation of a shallow stably stratified layer with high light availability are precisely the conditions that cause large phytoplankton blooms in lowland lakes [Kong et al., 2021]. Apart from contribution to the carbon and nutrients cycles, both the high radiation and the warm subsurface temperature may stimulate oxic methane production [Tang et al., 2016; Günthel et al., 2019] at levels significant to contribute to the greenhouse gas emissions to the atmosphere.

5 Conclusions

Our findings suggest that all freshwater (and apparently the majority of brackish) lakes on the Tibetan Plateau fully mix under ice, so that the convenient concept of winter stagnation, as known from traditional lake science, is inapplicable for these lakes. The 1-2 months long period of stable stratification at water temperatures above the maximum density value is an exceptional feature of high-altitude freshwaters. The resulting strong temperature gradient at the ice-water interface and a thin unstable layer right beneath intensify the heat flow from water to ice, making a crucial contribution to ice cover melting. The direct consequences of the deep convective mixing are aeration of the deep lake waters and upward supply of nutrients

to the upper photic layer, both suggesting versatile biogeochemical and ecological interactions specific for high-altitude lakes.

Acknowledgments

The study was a part of the research project "Lakes of Tibet as part of the Climate System" (LaTiCS) funded by the Sino-German Center for Research Promotion (CDZ project GZ1259) and by the German Research Foundation (DFG project KI 853/13-1). GK was additionally supported by the DFG grant KI 853/16-1. The data presented in the study will be made available by acceptance via the IGB Freshwater Research and Environmental Database (FRED) at https://fred.igb-berlin.de/

References

Barnes, D. F., and J. E. Hobbie (1960), Rate of melting at the bottom of floating ice, US Geol. Serv. Profess. Papers, 400, B392–B394.

Bengtsson, L., and T. Svensson (1996), Thermal regime of ice covered swedish lakes, Hydrology Research, 27(1-2), 39–56.

Biermann, T., W. Babel, W. Ma, X. Chen, E. Thiem, Y. Ma, and T. Foken (2014), Turbulent flux observations and modelling over a shallow lake and a wet grassland in the Nam Co basin, Tibetan Plateau, Theoretical and Applied Climatology, 116(1-2), 301–316.

Carlslaw, H. S., and C. S. Jaeger (1959), Conduction of Heat in Solids, 2nd ed., Oxford University Press, New York.

GLOBE Task Team (1999), The Global Land One-kilometer Base Elevation (GLOBE) Digital Elevation Model, Version 1.0., National Oceanic and Atmospheric Administration, National Geophysical Data Center, 325 Broadway, Boulder, Colorado 80305-3328, U.S.A., http://www.ngdc.noaa.gov/mgg/topo/globe.html accessed Mar 2021.

Golosov, S., O. Maher, E. Schipunova, A. Terzhevik, G. Zdorovennova, and G. Kirillin (2007), Physical background of the development of oxygen depletion in ice-covered lakes, Oecologia, 151(2), 331–340.

Günthel, M., D. Donis, G. Kirillin, D. Ionescu, M. Bizic, D. F. McGinnis, H.-P. Grossart, and K. W. Tang (2019), Contribution of oxic methane production to surface methane emission in lakes and its global importance, Nature communica-

tions, 10(1), 1–10.

Hersbach, H., B. Bell, P. Berrisford, S. Hirahara, A. Horányi, J. Muñoz-Sabater, J. Nicolas, C. Peubey, R. Radu, D. Schepers, et al. (2020), The era5 global reanalysis, Quarterly Journal of the Royal Meteorological Society, 146(730), 1999–2049.

Huang, W., J. Zhang, M. Leppäranta, Z. Li, B. Cheng, and Z. Lin (2019), Thermal structure and water-ice heat transfer in a shallow ice-covered thermokarst lake in central qinghai-tibet plateau, Journal of Hydrology, 578, 124,122.

Jakkila, J., M. Leppäranta, T. Kawamura, K. Shirasawa, and K. Salonen (2009), Radiation transfer and heat budget during the ice season in lake pääjärvi, finland, Aquatic Ecology, 43(3), 681–692.

Jerlov, N. G. (1976), Marine optics, Elsevier Oceanography Series 14, Elsevier, Amsterdam-Oxford-New York.

Kirillin, G., and A. Terzhevik (2011), Thermal instability in freshwater lakes under ice: Effect of salt gradients or solar radiation?, Cold Regions Science and Technology, 65(2), 184–190.

Kirillin, G., M. Leppäranta, A. Terzhevik, N. Granin, J. Bernhardt, C. Engelhardt, T. Efremova, S. Golosov, N. Palshin, P. Sherstyankin, G. Zdorovennova, and R. Zdorovennov (2012), Physics of seasonally ice-covered lakes: a review, Aquatic Sciences, 74(4), 659–682, doi:10.1007/s00027-012-0279-y.

Kirillin, G., A. Forrest, K. Graves, A. Fischer, C. Engelhardt, and B. Laval (2015), Axisymmetric circulation driven by marginal heating in ice-covered lakes, Geophysical Research Letters, 42(8), 2893–2900.

Kirillin, G., L. Wen, and T. Shatwell (2017), Seasonal thermal regime and climatic trends in lakes of the tibetan highlands, Hydrology and Earth System Sciences, 21(4), 1895–1909.

Kirillin, G., I. Aslamov, M. Leppäranta, and E. Lindgren (2018), Turbulent mixing and heat fluxes under lake ice: the role of seiche oscillations, Hydrology and Earth System Sciences, 22(12), 6493–6504.

Kong, X., M. Seewald, T. Dadi, K. Friese, C. Mi, B. Boehrer, M. Schultze, K. Rinke, and T. Shatwell (2021), Unravelling winter diatom blooms in temperate lakes using high frequency data and ecological modeling, Water Research, 190, 116,681.

Koźmiński, Z., and J. Wisznewski (1934), Über die Vorfrühlingthermik der Wigry-Seen, Archiv f. Hydrobiol., 28, 198–235.

Leppäranta, M., A. Terzhevik, and K. Shirasawa (2010), Solar radiation and ice melting in Lake Vendyurskoe, Russian Karelia, Hydrology Research, 41(1), 50–62.

Li, C., Y. Gong, T. Duan, Y. Zhu, L. Chen, and W. Li (2000), Observational study of super solar constant of the solar radiation over qinghai-tibet plateau, J. Chengdu Institute Meteorol, 15(2), 107–112.

Li, R., L. Zhao, Y. Ding, S. Wang, G. Ji, Y. Xiao, G. Liu, and L. Sun (2010), Monthly ratios of par to global solar radiation measured at northern tibetan plateau, china, Solar Energy, 84(6), 964–973.

Li, Z., S. Lyu, Y. Ao, L. Wen, L. Zhao, and S. Wang (2015), Long-term energy flux and radiation balance observations over Lake Ngoring, Tibetan Plateau, Atmospheric Research, 155, 13–25.

Lin, Z., F. Niu, H. Liu, and J. Lu (2011), Hydrothermal processes of alpine tundra lakes, Beiluhe basin, Qinghai-Tibet Plateau, Cold Regions Science and Technology, 65(3), 446–455.

Magnuson, J. J., D. M. Robertson, B. J. Benson, R. H. Wynne, D. M. Livingstone, T. Arai, R. A. Assel, R. G. Barry, V. Card, E. Kuusisto, et al. (2000), Historical trends in lake and river ice cover in the northern hemisphere, Science, 289(5485), 1743–1746.

Mironov, D., A. Terzhevik, G. Kirillin, T. Jonas, J. Malm, and D. Farmer (2002), Radiatively driven convection in ice-covered lakes: Observations, scaling, and a mixed layer model, Journal of Geophysical Research: Oceans, 107(C4).

Rossolimo, L. L. (1929), Thermik der Kossino-Seen, Trudy Kos. Biol. Stancii, 10, 3–49, (in Russian with German resume).

Su, F., L. Zhang, T. Ou, D. Chen, T. Yao, K. Tong, and Y. Qi (2016), Hydrological response to future climate changes for the major upstream river basins in the Tibetan Plateau, Global and Planetary Change, 136, 82–95, doi: 10.1016/j.gloplacha.2015.10.012.

Tang, K. W., D. F. McGinnis, D. Ionescu, and H.-P. Grossart (2016), Methane production in oxic lake waters potentially increases aquatic methane flux to air, Environmental Science & Technology Letters, 3(6), 227–233.

Terzhevik, A., S. Golosov, N. Palshin, A. Mitrokhov, R. Zdorovennov, G. Zdorovennova, G. Kirillin, E. Shipunova, and I. Zverev (2009), Some features of the thermal and dissolved oxygen structure in boreal, shallow ice-covered lake

vendyurskoe, russia, Aquatic Ecology, 43(3), 617–627.

Wang, M., J. Hou, and Y. Lei (2014), Classification of Tibetan lakes based on variations in seasonal lake water temperature, Chinese Science Bulletin, 59(34), 4847–4855, doi:10.1007/s11434-014-0588-8.

Wen, L., S. Lyu, G. Kirillin, Z. Li, and L. Zhao (2016), Air-lake boundary layer and performance of a simple lake parameterization scheme over the Tibetan highlands, Tellus A, 68(0), doi:10.3402/tellusa.v68.31091.

Zhang, G., T. Yao, H. Xie, J. Qin, Q. Ye, Y. Dai, and R. Guo (2014), Estimating surface temperature changes of lakes in the Tibetan Plateau using MODIS LST data, Journal of Geophysical Research: Atmospheres, 119(14), 8552–8567.

Пржевальский, Н. (1888), От Кяхты на истоки Желтой реки, исследование северной окраины Тибета и путь через Лоб-Нор по бассейну Тарима., 1 ed., Издание Имп. Русского Географического Общества, Санкт-Петербург.

Figure 1.

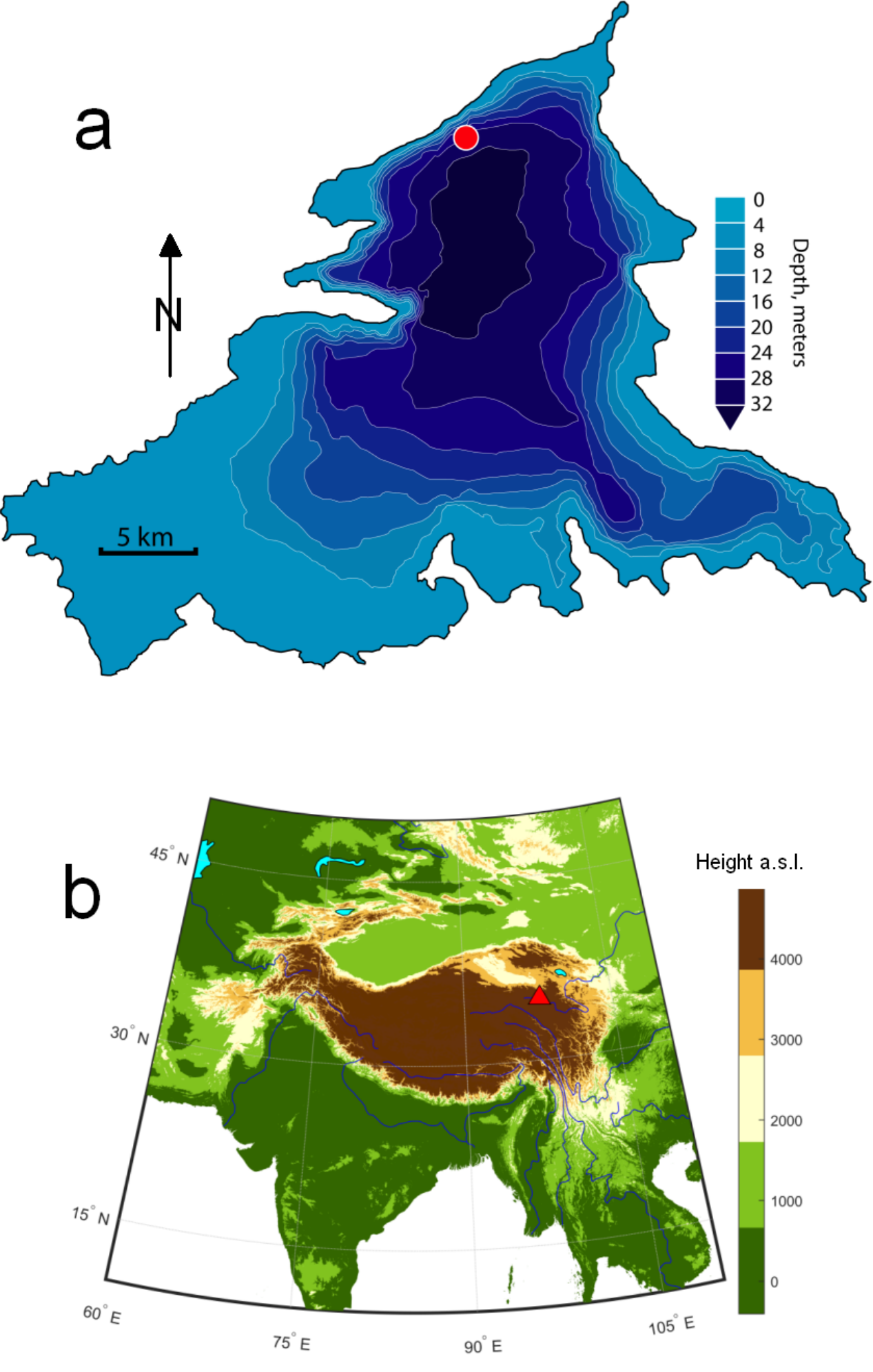
a
N
5 km
0
4
8
12
16
20
24
28
32
Depth, meters
b
45° N
30° N
15° N
60° E
75° E
90° E
105° E
Height a.s.l.
4000
3000
2000
1000
0

Figure 2.

a

Depth, m

0
5
10
15
20

Temperature, °C

0
1
2
3
4
5
6

1

2

b

T, °C

0
2
4
6
8
10

Partial ice cover (?):
24-Nov-2015

Ice On:
12-Dec-2015

"Mid-winter overturn":
04-Mar-2016

Ice Off:
18-Apr-2016

Mean Temperature
Surface Temperature
Bottom Temperature

Nov
Dec
Jan
Feb
Mar
Apr
May

Figure 3.

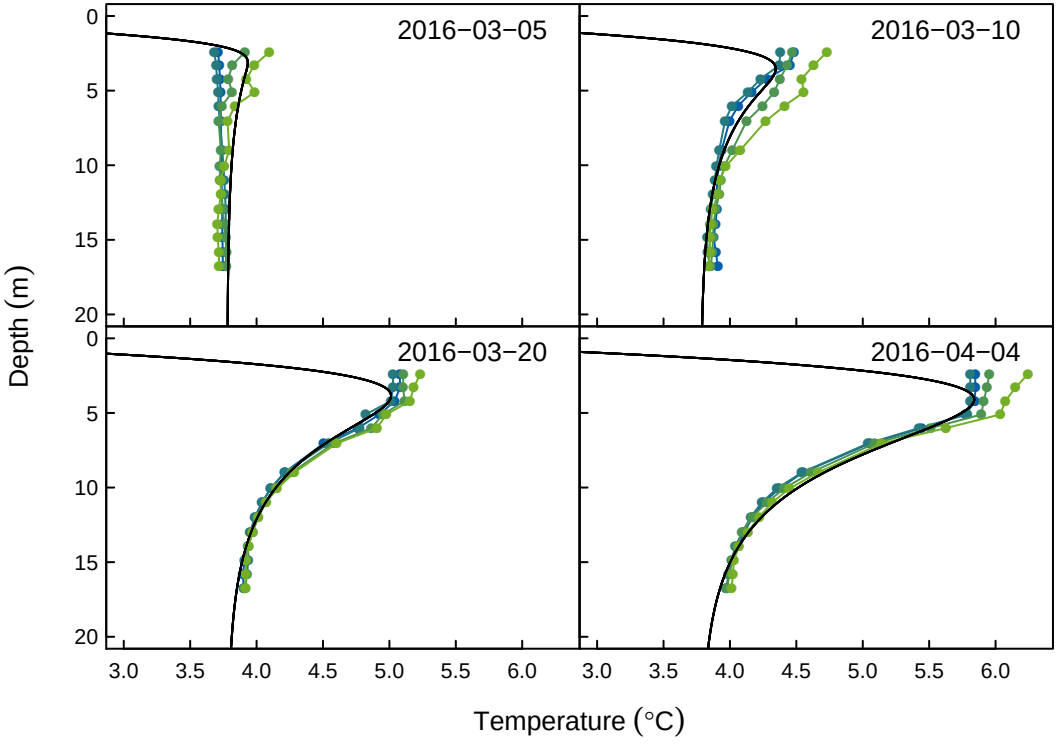
2016−03−05
2016−03−10
2016−03−20
2016−04−04
Depth (m)
0
5
10
15
20
3.0
3.5
4.0
4.5
5.0
5.5
6.0
Temperature (°C)

Figure 4.

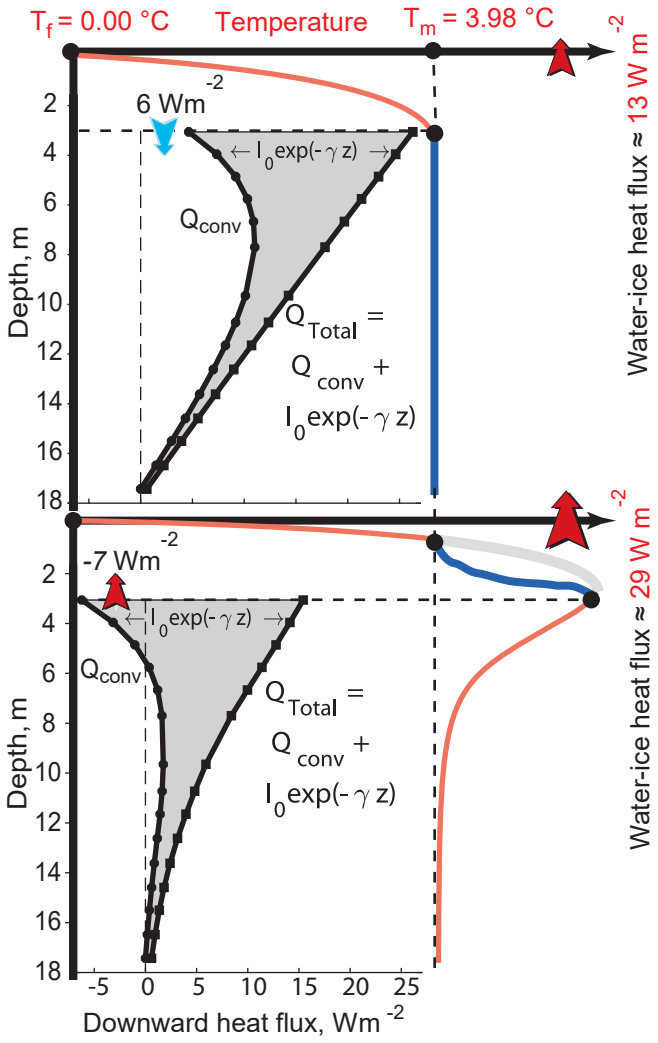
T_f = 0.00 °C
Temperature
T_m = 3.98 °C
6 Wm-2
← I0exp(-γ z) →
Qconv
QTotal = Qconv + I0exp(-γ z)
Water-ice heat flux ≈ 13 W m-2
-7 Wm-2
← I0exp(-γ z) →
Qconv
QTotal = Qconv + I0exp(-γ z)
Water-ice heat flux ≈ 29 W m-2
Depth, m
2
4
6
8
10
12
14
16
18
-5
0
5
10
15
20
25
Downward heat flux, Wm-2